

Interactions and screening in gated bilayer graphene nanoribbons

Hengyi Xu* and T. Heinzl

Condensed Matter Physics Laboratory, Heinrich-Heine-Universität, Universitätsstr.1, 40225 Düsseldorf, Germany

A. A. Shylau and I. V. Zozoulenko†

*Solid State Electronics, Department of Science and Technology,
Linköping University, 60174 Norrköping, Sweden*

(Dated: February 23, 2024)

The effects of Coulomb interactions on the electronic properties of bilayer graphene nanoribbons (BGNs) covered by a gate electrode are studied theoretically. The electron density distribution and the potential profile are calculated self-consistently within the Hartree approximation. A comparison to their single-particle counterparts reveals the effects of interactions and screening. Due to the finite width of the nanoribbon in combination with electronic repulsion, the gate-induced electrons tend to accumulate along the BGN edges where the potential assumes a sharp triangular shape. This has a profound effect on the energy gap between electron and hole bands, which depends nonmonotonously on the gate voltage and collapses at intermediate electric fields. We interpret this behavior in terms of interaction-induced warping of the energy dispersion.

PACS numbers: 81.05.Uw, 73.23.-b, 73.21.Ac

I. INTRODUCTION

Graphene and its bilayers are extremely good conductors with mobilities up to $20\text{m}^2/\text{Vs}$ at room temperature,^{1,2} which makes them interesting as active channels in field-effect transistors (FETs). These materials are also considered as building blocks for quantum electronics such as quantum computation and pseudospintronic devices.^{3–5} To facilitate these applications, large on-off resistance ratios are necessary.⁶ Several mechanisms for opening up an energy gap in two-dimensional (2D) monolayer graphene have been proposed to achieve this goal.⁷ It has been suggested that the application of an electric field between the two graphene layers breaks the inversion symmetry and induces an energy gap between electron and hole bands.⁸ Oostinga et al.⁹ have recently been able to detect such an electric-field induced energy gap in a graphene bilayer system. Infrared absorption spectroscopy furthermore demonstrated a gate-controlled band gap with gap energies up to 250 meV, which is in accordance with the self-consistent tight-binding calculations.^{10,11} The size of the gap is determined by the electric field between the two layers which can be tuned in single-¹² or double-¹³ gate geometries. Recently, the influence of a potential applied to a single gate on bilayer graphene has been studied theoretically within the continuum model, revealing a roughly linear dependence of the gap width as the carrier density increases.¹⁴ However, a nonmonotonous evolution of the gap width with the electron density has been predicted for graphene triple and quadruple layer systems, which has been attributed to trigonal warping of the band structure.^{15,16} Moreover, ab-initio density functional theory calculations have been used extensively to investigate the electronic structure of bilayer graphene and essentially confirm the behavior suggested by the tight-binding and continuum models.^{17–19}

Due to the presence of edges, graphene nanoribbons (GNRs) reveal a much richer phenomenology than 2D graphene sheets.^{20–22} GNRs possess energy gaps due to size quantization and edge states are formed with properties depending on the width and the type of edges.^{23,24} Edge disorder may result in transport gaps around the neutrality point.^{20,25–27} For gated GNRs, the electronic structure of monolayer systems has been modeled by Fernandez-Rossier with the image charge method in the Hartree approximation.²⁸ The inhomogeneous charge density and potential across the nanoribbons were found. Also, the small transverse size has a strong impact on the classical and quantum capacitances of monolayer GNRs.³¹

It is thus self-evident that interactions and imperfect screening should influence the electronic properties in bilayer GNRs (which we will refer to as BGNs below) as well and may modify the formation of the gate-voltage induced energy gap. However, neither the gate electrostatics, nor the self-consistent band structure and the band gap formation in BGNs (in contrast to bulk bilayers) have been studied before. In the present paper, we address this issue by taking Coulomb interactions in BGNs into account and studying the electron density distribution, the Hartree potential and the energy dispersion, focusing particularly on the evolution of the electric field induced band gap which can be regarded as a single-valued parameter for the relevance of the interaction effects.

The paper is organized as follows. In Sec. II we introduce the structure to be investigated and formulate our model. The results are presented and discussed in Sec. III. Sec. IV contains a summary and conclusions.

II. STRUCTURE AND MODEL

Throughout this work we consider long BGNs stacked in the Bernal form with ideal armchair edges. We note

$$\begin{aligned}
 H = & \sum_{\ell, \langle i, j \rangle} (V_{\ell, i} a_{\ell, i}^+ a_{\ell, i} + V_{\ell, j} b_{\ell, j}^+ b_{\ell, j}) - \gamma_0 \sum_{\ell, \langle i, j \rangle} (a_{\ell, i}^+ b_{\ell, j} + h.c.) \\
 & - \gamma_1 \sum_i (a_{1, i}^+ b_{2, i} + h.c.) - \gamma_3 \sum_{\langle i, j \rangle} (b_{1, i}^+ a_{2, j} + h.c.)
 \end{aligned} \tag{1}$$

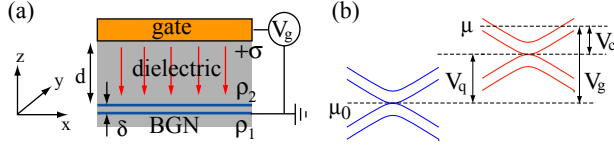


FIG. 1: (a) Scheme of the BGN device. The arrows indicate the direction of electric field for $V_g > 0$. (b) Illustration of the band structure shift induced by the gate voltage V_g , and of the voltage components V_c and V_q .

where $a_{\ell, i}^+$ ($b_{\ell, i}^+$) are the creation operators at sublattice A (B) in layer $\ell = 1, 2$ at site \mathbf{r}_i . We adopt the common graphite nomenclature and include the three coupling energies γ_0 , γ_1 and γ_3 , where $\gamma_0 = 3.16$ eV represents the intra-layer nearest-neighbor coupling energy, $\gamma_1 = 0.39$ eV is the coupling energy between sublattice B and A' in different graphene layers, and $\gamma_3 = 0.315$ eV the hopping energy between sublattice A and B' in the lower and upper layers, respectively. V_ℓ is the on-site potential arising from the Coulomb interaction of the induced charges the density of which is to be calculated.

In the capacitor structure shown in Fig. 1(a), a BGN of width w in y -direction and layer spacing $\delta = 0.335$ nm in z -direction extends along the x -direction and is embedded in an insulating medium (we assume a relative permittivity $\epsilon_r = 3.9$ adequate for SiO_2). The structure is covered by a homogeneous metallic gate extending in the xy -plane at distance d . Electrical access is enabled by connecting a voltage source to the metal gate and the lower BGN layer. A neutral BGN is obtained by setting the on-site potential to zero, corresponding to the Fermi energy $E_F = 0$. As a gate voltage V_g is applied, excess

charges $\rho_i = en_i$ are induced in the lower ($i=1$) and upper ($i=2$) graphene layer summing up to the total charge density $\rho = en$. Here, n_i denotes the carrier density in layer i and e the electron charge. This is balanced by the charge density σ of opposite polarity at the metal-oxide interface such that the Fermi energy departs from the neutrality point, while the charge neutrality of the whole system is conserved. In the following calculations, we subtract V_g from both the gate electrode as well as from the BGN which does not modify the electrostatics of the problem. This way, the gate metal-insulator interface is kept grounded which allows us to take advantage of the image charge technique creating a charge density at a distance d above the metal-insulator interface.²⁹

Within our framework, eV_g is defined as the difference between the electrochemical potential μ and the neutrality point of the discharged BGN μ_0 ,

$$eV_g = \mu - \mu_0, \tag{2}$$

see Fig. 1 (b) for an illustration. The displacement of the chemical potential is composed of the classical term eV_c associated with the electrostatic potential, and of the quantum term eV_q describing the accumulation of extra charges in the energy bands,

$$V_g = V_c + V_q. \tag{3}$$

The charge distribution screens the lateral electric field components at the gate. Taking the Coulomb interactions between the charges and their images into account, the Hartree potential at the site \mathbf{r} in the continuous limit can be computed as

$$V(\mathbf{r}(x, y)) = -\frac{e}{4\pi\epsilon_0\epsilon_r} \int dy' \rho(y') \left(\ln \frac{(y-y')^2}{(y-y')^2 + 4(d+\xi\delta)^2} + \ln \frac{(y-y')^2 + \delta^2}{(y-y')^2 + (2d+\delta)^2} \right) \tag{4}$$

with $\xi = 1$ and 0 for the lower and the upper layer of the BGN, respectively. The first term describes the interac-

tion between the charges in each layer and their corre-

sponding mirror charges, while the second term accounts for the interaction of the charges in one layer with the mirror charges related to the other layer.

In order to determine the charge density, the local density of states $D(r, E)$ (LDOS) at site r and energy E is calculated with the help of the real-space Green's functions technique described in Ref. 35. The electron density at site r is then given by

$$n(r) = \int_{-\infty}^{\mu} D_{sc}(E) f(E) dE - \int_{-\infty}^{\mu_0} D_0(E) f(E) dE \quad (5)$$

where $f(E)$ is the Fermi-Dirac distribution. $D_{sc}(E)$ and $D_0(E)$ represent the LDOS at energy E with and without including the self-consistent interactions, respectively. In the actual calculations, the second term is replaced by $4/\sqrt{3}a^2$ with $a = 0.246$ nm which represents the positive charge background of the ions. Since the Hartree potential, Eq. (4) depends on $n(r)$ which is a solution of the Schrödinger equation with the Hamiltonian given by Eq.

(1), these equations are solved by the Broyden iterative method.

Some insight into the basic physics of gated BGNs is obtained from the analytical expression for the potential difference between the layers induced by gate voltage. Since $\delta \ll d$, we can approximate the BGN by a conducting strip with the total charge density ρ . The relation between gate voltage and the charge density for the system formed between the conducting strip of width w located at the distance d apart from a semi-infinite plate is given by³¹

$$V_g = \frac{\rho}{\pi\epsilon_0\epsilon_r} \left[2d \arctan\left(\frac{w}{4d}\right) + \frac{w}{4} \ln \left\{ 1 + \left(\frac{4d}{w}\right)^2 \right\} \right] \quad (6)$$

The potential difference between the graphene layers can be calculated by integrating the electric field in between, i.e., $\Delta V = \int_d^{d+\delta} E(z) dz$. By using the method of image charges, one finds that $E(z)$ is determined by

$$E(z) = E_{\rho_2}^{strip}(z+d) + E_{\rho_1}^{strip}(z+(d+\delta)) + E_{-\rho_2}^{strip}(z-d) + E_{-\rho_1}^{strip}(z-(d+\delta)) \quad (7)$$

where the first two terms in the summation correspond to the image charges. The intensity of the electric field at distance z from the middle of a strip is given by³¹

$$E_{\rho}^{strip}(z) = \frac{\rho}{\pi\epsilon_0\epsilon_r} \arctan\left(\frac{w}{2z}\right) \quad (8)$$

Performing the integration and using Eqs. (6)-(8), we get

$$\Delta V = \frac{\delta \arctan\left(\frac{w}{4d}\right) V_g}{\left[2d \arctan\left(\frac{w}{4d}\right) + \frac{w}{4} \ln \left\{ 1 + \left(\frac{4d}{w}\right)^2 \right\} \right]} - \frac{\Delta\rho}{2\epsilon_0\epsilon_r} \quad (9)$$

where $\Delta\rho = \rho_2 - \rho_1$ is the charge density difference. In the derivation of Eq. (9), a homogeneous distribution of the charge density in the BGN has been assumed. This assumption is a reasonable approximation for low charge densities.

III. RESULTS AND DISCUSSION

Figs. 2(a) and (b) show the electron density distributions and Hartree potentials of BGN with $N = 49$ sites in transverse direction, corresponding to $w = 12$ nm for different gate voltages. The calculations are performed over one unit cell containing $4N$ sites. To clarify the role of electron-electron interactions we show the self-consistent Hartree (right parts) and non-interacting (left parts) calculations. In our context, non-interacting calculations correspond to the Hamiltonian (1) where the

potential difference between the layers is given by Eq. (9) with $\Delta\rho$ set to 0. Both non-interacting and self-consistent calculations show pronounced oscillations between neighboring sites. Because of this we also plot for clarity the density distributions averaged over six neighboring sites. Within the self-consistent treatment, the electrons tend to accumulate along the edges as a manifestation of electronic repulsion. As the gate voltage is increased, the edge accumulation becomes more prominent. It is worth pointing out that it is primarily the applied gate voltage which determines this distribution, resembling that one found in monolayer GNRs.^{30,31} This edge accumulation is reflected in the Hartree potential as the formation of triangular-shaped wells near the edges, an effect known in quantum wires prepared by cleaved-edge overgrowth³² as well as from wide two-dimensional quantum wells³³. In the non-interacting case, on the other hand, the charge density distributions which are obtained by using the potential profiles in the left panels are quite flat, while the electron density oscillations between neighboring sites persist.

For comparison, we also plot the electron density and potential of a monolayer GNR of identical width. The constant potentials shown in the left panels are classical responses of the BGN to the gate voltage corresponding to the position of the charge neutrality point V_c . The BGN system can be viewed as two monolayer GNRs connected in series such that the classical capacitance of the BGN is smaller than that of monolayer GNR, resulting in larger values of V_c . Comparing the averaged electron

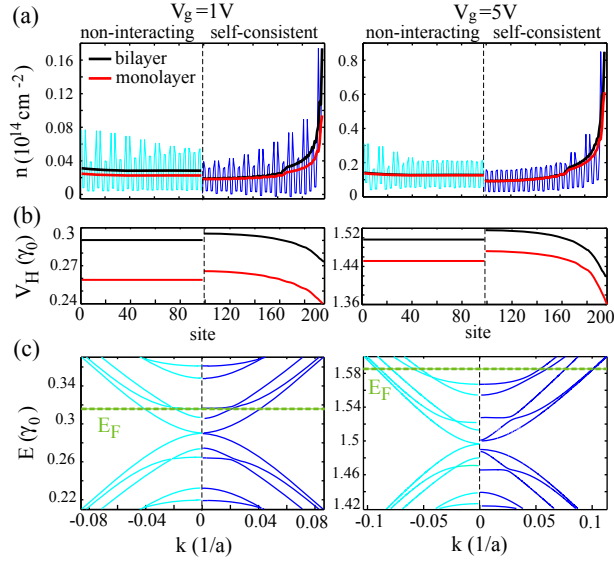


FIG. 2: Comparison between the single-particle (left parts) and the self-consistent Hartree (right parts) calculations for different gate voltages. The distance between the gate and the BGN is set to $d = 100 \text{ nm}$. (a) Induced electron density distribution along the y direction (thin lines) and the values averaged over six neighbors (bold lines). (b) Potential profiles from the one-electron and the Hartree approximation calculations, averaged over six neighbors. (c) Band structures. The dashed horizontal lines indicate the Fermi level.

density, one finds that they are very close at the center of nanoribbons in both cases, which is consistent with the fact that the total induced charge density equals to the sum of the densities in each layer, i.e., satisfying the relation $\sigma = -(\rho_1 + \rho_2)$ according to electrostatics for bilayer. There are however some small differences close to edges which we interpret as a consequence of interlayer Coulomb interactions.

Fig. 2(c) shows the dispersion relations of $V_g = 1\text{V}$ and 5V for the non-interacting and self-consistent cases. Within the single-particle picture, the potential energy across the BGN is constant and the dispersion relations are shifted upwards almost rigidly as the gate voltages increase. The energy gaps induced by the gate voltage are barely visible. Turning on the electronic interactions, the potential profile changes only slightly for $V_g = 1\text{V}$. However, as the gate voltage increases to 5V , the dispersion relation gets strongly modified. Anticrossings are generated and a significant energy gap is opened between the conduction and valence bands, originating not only from the potential difference between the layers but also from the transverse potential profile. We note in this respect that even in monolayer GNRs, the external electric field can lead to a gap modulation for semiconductor armchair nanoribbons³⁶ and to a gap opening for zigzag ribbons³⁷.

We continue by considering the average electron density and the Hartree potential in each graphene layer as a function of the gate oxide thickness d . As shown in Fig. 3(a), the electron densities in both layers increase

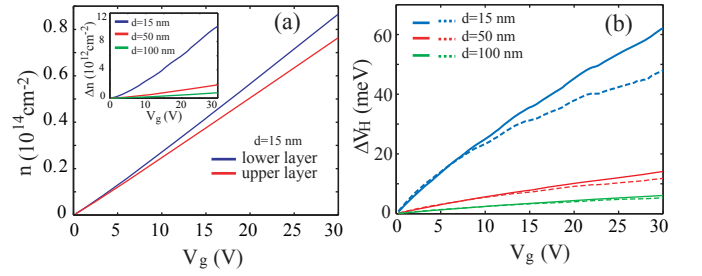


FIG. 3: (a) The average electron density on each graphene layer for dielectric thickness $d = 15 \text{ nm}$. Inset: The difference of the average density between layers for different dielectric thicknesses. (b) The difference of Hartree potentials between graphene layers. Solid and dashed lines correspond to the numerical and analytical calculations from Eq. (9), respectively.

approximately linearly V_g . In monolayer GNRs, a similar linear relation of electron density and gate voltage $\rho \propto V_g$ has been reported.²⁸ This common feature indicates that the classical electrostatic contribution predominantly determines the charge density. Furthermore, the electron densities of the two layers of the BGN diverge as the gate voltage increases. This electron density difference grows monotonously as shown in the inset. The dependence of the potential differences on d is basically governed by the classical component. Fig. 3(b) shows the corresponding results of the Hartree potential. The analytical expression according to Eq. (9) quantitatively reproduces the exact numerical results at the low gate voltages, especially for larger dielectric thickness $d = 50 \text{ nm}$ and 100 nm . However, deviations emerge for higher gate voltages, most pronounced for $d = 15 \text{ nm}$. They can be understood via the derivation of Eq. (9), which is based on the assumption that induced electron density is homogeneous and the potential across the ribbon is constant. In reality, both a larger V_g and a smaller d lead to the higher electron densities, stronger Coulomb repulsion and more pronounced potential inhomogeneities, rendering the classical capacitor approximation less valid.

We proceed with a detailed study of the effects of Coulomb interactions on the band structures, and begin with looking at the size of the energy gap as a function of the gate voltage for different dielectric thicknesses as shown in Fig. 4(a). In contrast to the 2D bilayer graphene, where the band gap increases monotonously as the applied electric field is increased,¹⁰ the energy gap in BGNs exhibits a pronounced dip at low gate voltages for all values of d . If the single-particle potential is used instead, the energy gap increases monotonously with V_g and follows closely the value of the Hartree potential difference shown in Fig. 3(b), and the dip is absent. This implies that the interactions are responsible for the formation of the dips. To shed light on the origin of this suppression of the band gap formation, let us inspect the band structures for $d = 15 \text{ nm}$ at several representative Fermi energies. For the first two selected values of V_g , ① and ②, the size of gap is proportional to V_g . One

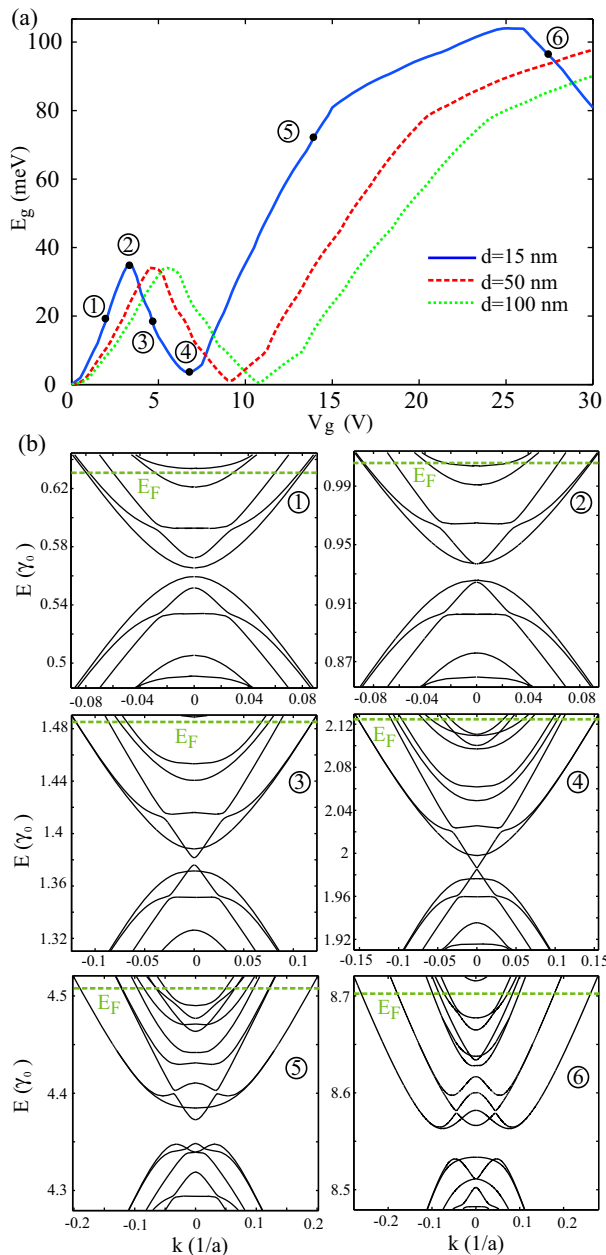


FIG. 4: (a) The energy gap as a function of the applied gate voltage for various dielectric thicknesses d . (b) Representative band structures corresponding to the Fermi energies shown in (a). The dashed lines indicate the positions of Fermi energy.

observes that the second energy band of the electrons develops an anticrossing with the third one and develops a strong curvature around $k_x = 0$. The minimum of this band approaches the conduction band edge formed by the lowest energy band and takes over the role of the band edge at the scenarios depicted in Figs. 4(b), ③ and ④. As a result, the energy gap gets reduced as the gate voltage increases and can even approach zero for some parameters. We note that a similar effect has been discussed by Avetisyan et al., in graphene tri- and

quadruple-layer systems based on a different mechanism, however.¹⁵ As the voltage is increased beyond the dip of the energy gap (e.g. $V_g \gtrsim 25$ for $d = 15$ nm), the familiar Mexican hat shaped dispersion emerges which leads to the reduction of the energy gap while the electron-hole symmetry vanishes.

From this evolution of the energy band dispersions, it becomes apparent that the Hartree term induces some warping of the energy dispersion. We note that in contrast to 2D bilayer systems,³⁸ this effect is not due to γ_3 , since after setting $\gamma_3 = 0$ the band structure changes only slightly but the collapse of the band gap persists (not shown here). The prerequisite for is the potential inhomogeneity generated by the charge accumulation at the edges. This is why the collapse of the band gap is absent in the 2D cases. Furthermore, the small reduction of the energy gap for large V_g in the system with $d = 15$ nm is not directly related to warping but is the result of the Mexican-hat band formation.

IV. SUMMARY AND CONCLUSIONS

We have studied the electron density distribution and Hartree potential of a single-gated BGN. Coulomb interactions are incorporated in a self-consistent way within the Hartree approximation. The repelling electrons accumulate at the BGN edges and induce characteristic dips in the transverse potential profile. They change the band structures strongly and modify the energy gaps which thereby behave qualitatively differently compared to 2D bilayer systems, showing an unusual reduction in the sizes of the energy gaps at intermediate gate voltages. An analytical expression for the potential difference between the two layers is obtained based on the assumption of a classical capacitor and compared with self-consistent numerical calculations. They show good agreement at small gate voltages. The discrepancies found at higher voltages and small dielectric thicknesses are due to the assumption of homogeneous charge density and constant potential in the analytical model. This becomes invalid for high electron densities because the quantum mechanical effects modify the charge redistribution significantly. A disadvantage of the single-gate structure discussed here is that due to small capacitance, the Fermi energy is far above the neutrality point in the regime of the collapse of the band gap, such that this effect is not directly accessible experimentally. This shortcoming can conceptually be overcome by performing corresponding simulations for a double-gate structure, where independent tuning of the Fermi energy and the interlayer electric field is possible.^{9,13}

Acknowledgments

H.X. and T.H. acknowledge financial support from Heinrich-Heine-Universität Düsseldorf and the German

Academic Exchange Service (DAAD) within the DAAD-STINT collaborative grant. A.A.S. and I.V.Z. acknowledge the support from the Swedish Research Council

(VR) and from the Swedish Foundation for International Cooperation in Research and Higher Education (STINT) within the DAAD-STINT collaborative grant.

-
- * Electronic address: hengyi.xu@uni-duesseldorf.de
† Electronic address: igor.zozoulenko@itn.liu.se
- ¹ S. V. Morozov, K. S. Novoselov, M. I. Katsnelson, F. Schedin, D. C. Elias, J. A. Jaszczak, and A. K. Geim, *Phys. Rev. Lett.* **100**, 016602 (2008).
 - ² J. Chen, C. Jang, S. Xiao, M. Ishigami, and Michael S. Fuhrer, *Nature Nanotech.* **3**, 206 (2008).
 - ³ M. I. Katsnelson, K. S. Novoselov, and A. K. Geim, *Nat. Phys.* **2**, 620 (2006).
 - ⁴ B. Trauzettel, D. V. Bulaev, D. Loss and G. Burkard, **3**, 192 (2007).
 - ⁵ P. San-Jose, E. Prada, E. McCann, and H. Schomerus, *Phys. Rev. Lett.* **102** 247204 (2009).
 - ⁶ Vitor M. Pereira and A. H. Castro Neto, *Phys. Rev. Lett* **103**, 046801 (2009).
 - ⁷ R. N. Costa Filho, G. A. Farias, and F. M. Peeters, *Phys. Rev. B* **76**, 193409 (2007).
 - ⁸ E. McCann and V. I. Fal'ko, *Phys. Rev. Lett.* **96** 086805 (2006).
 - ⁹ J.B. Oostinga, H.B. Heersche, X. Liu, A.F. Morpurgo, and L.M.K. Vandersypen, *Nat. Mat.*, **7**, 151 (2007).
 - ¹⁰ Y. Zhang, T. Tang, C. Girit, Z. Hao, M. C. Martin, A. Zettl, M. F. Crommie, Y. R. Shen, F. Wang, *Nature (London)* **459**, 820 (2009).
 - ¹¹ K. F. Mak, C. H. Lui, J. Shan, and T. F. Heinz, *Phys. Rev. Lett.* **102**, 256405 (2009).
 - ¹² F. Xia, D. B. Farmer, Y. Lin, and P. Avouris, *Nano. Lett.* **10**, 715 (2010).
 - ¹³ M. Koshino and E. McCann, *Phys. Rev. B* **79**, 125443 (2009).
 - ¹⁴ E. McCann, *Phys. Rev. B* **74**, 161403(R) (2006).
 - ¹⁵ A. A. Avetisyan, B. Partoens, and F. M. Peeters, *Phys. Rev. B* **79**, 035421 (2009).
 - ¹⁶ A. A. Avetisyan, B. Partoens, and F. M. Peeters, *Phys. Rev. B* **80**, 195401 (2009).
 - ¹⁷ H. Min, B. Sahu, S. K. Banerjee, and A. H. MacDonald, *Phys. Rev. B* **75**, 155115 (2007).
 - ¹⁸ E. K. Yu, D. A. Stewart, S. Tiwari, *Phys. Rev. B* **77**, 195406 (2008).
 - ¹⁹ P. Gava, M. Lazzeri, A. Marco Saitta, and F. Mauri, *Phys. Rev. B* **79**, 165431 (2009).
 - ²⁰ M. Y. Han, B. Ozyilmaz, Y. Zhang, and P. Kim, *Phys. Rev. Lett.* **98**, 206805 (2007).
 - ²¹ X. Wang, Y. Ouyang, X. Li, H. Wang, J. Guo, and H. Dai, *Phys. Rev. Lett.* **100**, 206803 (2008).
 - ²² D. A. Areshkin, D. Gunlycke, and C. T. White, *Nano. Lett.* **7**, 204 (2007).
 - ²³ K. Wakabayashi, M. Fujita, H. Ajiki, and M. Sgrist, *Phys. Rev. B* **59**, 8271 (1999).
 - ²⁴ K. Nakada, M. Fujita, G. Dresselhaus, and M. S. Dresselhaus, *Phys. Rev. B* **54**, 17954 (1996).
 - ²⁵ M. Evaldsson, I. V. Zozoulenko, Hengyi Xu, and T. Heinzl, *Phys. Rev. B* **78**, 161407(R) (2008).
 - ²⁶ Hengyi Xu, T. Heinzl, and I. V. Zozoulenko, *Phys. Rev. B* **80**, 045308 (2009).
 - ²⁷ E. R. Mucciolo, A. H. Castro Neto, and C. H. Lewenkopf, *Phys. Rev. B* **79**, 075407 (2009).
 - ²⁸ J. Fernandez-Rossier, J.J. Palacios, and L. Brey, *Phys. Rev. B* **75**, 205441 (2007).
 - ²⁹ N. M. R. Peres, J. N. B. Rodrigues, T. Stauber, and J. M. B. Lopes dos Santos, *J. Phys. Condens. Matt.* **21**, 344202 (2009).
 - ³⁰ P. G. Silvestrov and K. B. Efetov, *Phys. Rev. B* **77**, 155436 (2008).
 - ³¹ A. A. Shylau, J. W. Klos, and I. V. Zozoulenko, *Phys. Rev. B* **80**, 205402 (2009).
 - ³² S. Ihnatsenka and I. V. Zozoulenko, *Phys. Rev. B* **74**, 075326 (2006).
 - ³³ Y. W. Suen, J. Jo, M. B. Santos, L. W. Engel, S. W. Wang, and M. Shayegan, *Phys. Rev. B* **44**, 5947 (1991).
 - ³⁴ A. H. Castro Neto, F. Guinea, N.M.R. Peres, K.S. Novoselov, and A. K. Geim, *Rev. Mod. Phys.* **81**, 109 (2009).
 - ³⁵ Hengyi Xu, T. Heinzl, M. Evaldsson, and I.V. Zozoulenko, *Phys. Rev. B* **77**, 245401 (2008).
 - ³⁶ C. Ritter, S.S. Makler, and A. Latg, *Phys. Rev. B* **77**, 195443 (2008).
 - ³⁷ Y.-W. Son, M.L. Cohen, and S.G. Louie, *Nature (London)* **444**, 347 (2006).
 - ³⁸ M. Koshino, *New J. Phys.* **11**, 095010 (2009).